AIP Conference Proceedings

RESEARCH ARTICLE | OCTOBER 06 2023

A comparison between model predictive and PID-based control of a molten salt solar tower receiver

Rudolf Popp ✉; Kevin Iding; Peter Schwarzbözl; Thomas Konrad; Dirk Abel

Check for updates

AIP Conf. Proc. 2815, 030016 (2023)
https://doi.org/10.1063/5.0148728

View Online Export Citation CrossMark

27 February 2024 08:50:56

AIP Advances
Why Publish With Us?
25 DAYS average time to 1st decision
740+ DOWNLOADS average per article
INCLUSIVE scope
Learn More
AIP Publishing

AIP Publishing

A Comparison Between Model Predictive and PID-Based Control of a Molten Salt Solar Tower Receiver

Rudolf Popp[1, a)] and Kevin Iding[2] and Peter Schwarzbözl[2] and Thomas Konrad[1] and Dirk Abel[1]

[1]*Institute of Automatic Control, RWTH Aachen University, Campus-Boulevard 30, 52074 Aachen, Germany*
[2]*Institute of Solar Research, German Aerospace Center, Linder Höhe, 51147 Cologne, Germany*

[a)] Corresponding author: r.popp@irt.rwth-aachen.de

Abstract. In this paper a model predictive control (MPC) for operating a solar tower receiver is evaluated and compared with the performance of a PID-based control, that is considered as conventional control approach. The receiver outlet temperature is controlled by the mass flow, while the solar irradiance is considered as measurable disturbance. The control algorithms are tested via simulation on a virtual power plant based on a high-fidelity model of the receiver. For carrying out the evaluations, 24 validation cases are evaluated in terms of control error and compliance with limits for a high durability of receiver. As a result, the MPC has the potential to operate a solar tower molten salt receiver in a secure and optimal way as well as to increase the degree of automation.

27 February 2024 08:50:56

INTRODUCTION

Among Concentrated Solar Power (CSP) systems, solar towers using molten salt as heat transfer fluid (HTF) show the potential to be technically and economically superior [1]. Due to high incident flux densities on the receiver, solar towers can operate at high temperatures and enable high efficiencies. At the same time, these high thermal loads pose challenges on the process control since the temperature constraints of the material need to be considered. The HTF must be kept within a temperature range between solidification (approx. 220°C) and decomposition (approx. 600°C) at any location in the receiver. Especially during transient operation due to cloud passages, the rapid increase of the irradiated power can lead to violation of the allowable flux densities (AFD) and temperature limits, resulting in direct damage and reduced life time of the receiver system [2].

For CSP systems different control strategies have been developed and tested. Especially to parabolic trough power plants, control purposes like feed forward controllers [3], nonlinear feedback linearization [4] or model predictive control (MPC) with different variations [5] have been applied. For solar tower systems, the control concept is typically composed of two stages: The heliostat field and the mass flow control of the HTF. While the major development focuses on the complex problem of manipulating the flux density, the mass flow is generally controlled by a conventional feedforward PID controller, that was already proposed in the solar two project, one of the first demonstrator solar tower plants for the technology with molten salt receivers [6]. To control the temperature of a molten salt receiver, Bertinho et al. [7] present a Lyapunov based controller that results in an explicit control law with a nonlinear feedforward term considering the solar irradiance and a state feedback term.

In this paper, a MPC is proposed that explicitly considers the limits for safe operation and controls the outlet temperature to the desired set point. Contrary to [7], the control law is implicit and calculated by solving an optimal control problem iteratively. For this study, the heliostat field is assumed to be operated with an optimized aim-point distribution for the clear-sky situation. This aim-point distribution was optimized in advance by a ray tracing tool [8], and meets the flux limits for quasi-stationary clear sky operation in 5 min time steps. Deviations from the clear-sky

SolarPACES: Solar Power & Chemical Energy Systems
AIP Conf. Proc. 2815, 030016-1–030016-8; https://doi.org/10.1063/5.0148728
Published by AIP Publishing. 978-0-7354-4623-6/$30.00

scenario (through clouds) lead to changes of the flux density on the receiver which the MPC treats as disturbance and uses the mass flow as manipulated variable. This paper compares the control performance of the solar tower receiver between an MPC and a conventional PID-based controller that is currently widely used for solar tower power plants. The paper is organized as follows: First, a system overview is given, and the control problem is motivated. Then, a brief design of the PID controller and the MPC is presented, before the defined test scenarios are introduced. On this basis, the control strategies are evaluated. Eventually a conclusion is given.

SYSTEM OVERVIEW

The developed MPC is tested on a virtual power plant, which is a reference system for a typical power plant with molten salt receiver. The receiver design is defined using data from the company General Electric (GE). The parameters, shown in Table 1, were chosen for the reference plant.

TABLE 1. Design parameters of the reference power plant

Location	South Africa (28.3 ° south)
Design point	21.03., solar noon
Thermal power in design point	650 MW_{th}
Mass flow in design point	1560 kg/s
Temperature set point	565 °C
Reflected area by heliostat field	1 335 000 m^2
Receiver area	1 421 m^2
Number of panels per branch	17

According to this design, the receiver is modelled in a commercial modelling simulation environment (Dymola), based on the work of [9]. Figure 1 displays the principal sketch of the system. The cylindrical receiver at the top of the tower consists of a system of parallel and serial arranged pipes through which the molten salt flows in a meandering manner via two paths around the receiver. Reflected by the heliostat field, the solar irradiance is concentrated onto the outer surface of the receiver pipes and heats up the molten salt.

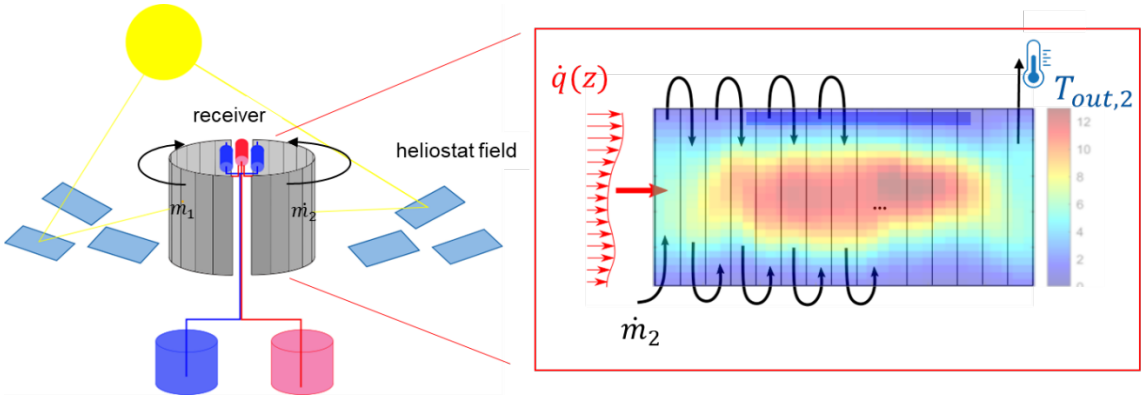

FIGURE 1. Principle sketch and components of the solar tower plant

The environment of the receiver is modelled by the Solar Tower Raytracing Laboratory (STRAL) [5] that simulates the cloud passage and the behavior of the heliostat field, while keeping the heliostat aim-point allocation according to the precalculated clear-sky solution. For this reason, the reference point optimization is also carried out by STRAL and is not part of the MPC. As a result, the irradiance distribution $\dot{q}(z)$ is considered as measurable disturbance, while the mass flowrates $\dot{m}_1$ and $\dot{m}_2$ of the molten salt are the only manipulated variables for controlling the output temperatures $T_{\mathrm{out},1}$ and $T_{\mathrm{out},2}$ to a set point temperature of 565 °C. Additionally, the salt temperature can be measured at each panel output. The limits for the absorbed flux density are due to material stresses and a specification of the receiver manufacturer (GE). Figure 2 shows these limitations for different mass flowrates and pipe types. They are defined by the allowable flux density (AFD) that was introduced by [2]. The AFD depends on the mass flow, the salt temperature and the panel material. In this receiver by GE, two different materials are used.

27 February 2024 08:50:56

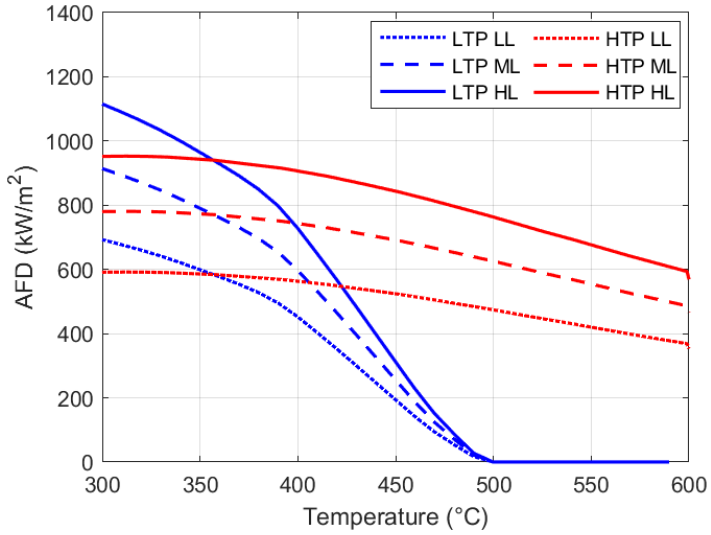

FIGURE 2. Allowable flux densities due to pipe stresses for three different mass flows and two different panel types (Low Temperature Panel: LTP, High Temperature Panel: HTP, Low Load-LL, Medium Load-ML and High Load-HL).

For the salt, temperature limits are specified in the average (bulk) as well as in the peak (film), that have to be maintained at any location in the receiver (Table 2). Since the film temperatures have a higher dynamic behavior due to the lower thermal capacity of the pipe, they are more critical for salt degradation. Therefore, it is sufficient to consider only film temperatures limits by the MPC to keep the salt in safe operation range.

27 February 2024 08:50:56

TABLE 2. Limits for the salt temperature. The stationary limit can be violated for a maximum of 5 minutes. The transient limit must never be violated.

Type of limit	Max. temperatures	
	Bulk in °C	Film in °C
Stationary (max. 5 min.)	580	600
Transient	602	616

CONTROL ALGORITHM

The feedforward- PID controller consist of parallel coupled feedforward and feedback paths. The feedforward term uses the flux density and computes mass flow that is needed to reach the set temperature under steady state conditions. The receiver outlet temperature is used as feedback to manipulate the mass flow with a proportional, integral and differential (PID) term. The parameters were initially designed according to the rules of Chien, Hrones and Reswick [11] and eventually carefully adapted based on step responses to react as fast as possible with little overshoot. To protect the receiver from overheating during a rapid rise after a cloud passage, the cloud standby mode overlays the controller. This mode is activated, if the receiver outlet temperature drops below 510 °C.

The MPC internally uses a reduced-order model [10] to predict the future plant behavior. Using a forecast of the incident irradiance is possible, but is not considered here because knowing the exact forecast would not be realistic. Instead, the current irradiance is assumed to be constant in future. The MPC controls the receiver in terms of the defined cost function J, which describes a desired behavior of the receiver in a considered time window, the prediction horizon of length N_H. A deviation from the desired behavior results in an increase of the costs. The goal of the MPC is to find a control variable sequence $\{\dot{m}_0 \dots \dot{m}_{\mathrm{N_p}}\}$ by a mathematical optimization, which minimizes the cost function.

In equation (1) the cost function is defined to penalize

- the deviation of the output temperature T_{out} from the set point temperature $r = 565\ °C$ with a function $l(r, T_{\mathrm{out}})$,
- the change of the manipulated variable to gain a smooth control behavior and avoid oscillations,
- and the violation of the restricted variables by the slack variables $\boldsymbol{s} = \{\boldsymbol{s}_{\mathrm{film}},\ \boldsymbol{s}_{\mathrm{afd}}\}$. The slack variables are introduced to transfer these mathematical strong limitations into soft constraints. If the solution of the optimal problem might get infeasible, small violations of the soft constraints are allowed.

The weighting parameters $\boldsymbol{Q}_{\mathrm{r}}, \boldsymbol{Q}_{\mathrm{f}}, \boldsymbol{Q}_{\mathrm{afd}}$ and $\boldsymbol{R}$ are designed to prioritize the individual control objectives against each other. The optimization task is subjected to the discrete system dynamics $F(\boldsymbol{x}(k), \dot{\boldsymbol{q}}(k),\ u(k))$ and the operational constraints of the manipulated variables (equations (3) and (4), where $\dot{m}_{\mathrm{max}}$ is the mass flowrate in the design point and $\boldsymbol{x}$ the state space variable.

$$\min_{\substack{\dot{m}_0 \dots \dot{m}_{\mathrm{N_u}} \\ \boldsymbol{s}_0 \dots \boldsymbol{s}_{\mathrm{N_P}}}} J = \sum_{k=0}^{N_p} l(r_{\mathrm{k}} - T_{\mathrm{out}}(\cdot\,|k), \boldsymbol{Q}_{\mathrm{r}}) + \| \boldsymbol{s}_{\mathrm{film}}(\cdot\,|k) \|^2_{\boldsymbol{Q}_{\mathrm{f}}} + \| \boldsymbol{s}_{\mathrm{afd}}(\cdot\,|k) \|^2_{\boldsymbol{Q}_{\mathrm{afd}}} + \sum_{k=0}^{N_{\mathrm{u}}} \| \Delta \dot{m}(\cdot\,|k) \|^2_{\boldsymbol{R}} \tag{1}$$

$$\text{s.t.} \qquad \dot{\boldsymbol{x}}(k+1) = F(\boldsymbol{x}(k), \dot{\boldsymbol{q}}(k),\ u(k)) \tag{2}$$

$$-0{,}2\ \dot{m}_{\mathrm{max}} < \Delta u < 0{,}2\ \dot{m}_{\mathrm{max}} \tag{3}$$

$$0{,}2\ \dot{m}_{\mathrm{max}} < u < 1{,}1\ \dot{m}_{\mathrm{max}} \tag{4}$$

$$\boldsymbol{T}_{\mathrm{film}} - \boldsymbol{s}_{\mathrm{film}} < \boldsymbol{T}_{\mathrm{film,limit}} \tag{5}$$

$$\dot{\boldsymbol{q}}_{\mathrm{abs}} - \boldsymbol{s}_{\mathrm{afd}} < afd(\boldsymbol{x}(k), \dot{m}(k)) \tag{6}$$

$$\boldsymbol{s}_{\mathrm{film}} \geq 0 \tag{7}$$

$$\boldsymbol{s}_{\mathrm{afd}} \geq 0 \tag{8}$$

VALIDATION ON VIRTUAL CLOUD PASSAGE SCENARIOS

The behavior of the controlled system is largely dependent on the solar irradiation of the heliostat field, as well as the temporal and spatial distribution, which essentially results from the position of the sun and the cloud situation. To validate the control concept, 32 scenarios were defined considering a cloud passage of one-hour duration. All scenarios were simulated on a March 21st, since this date results in an average elevation angle related to the entire year. Figure 3 shows the averaged incident flux density on both branches A and B for some parameter variations. The scenarios were defined by varying

- day-time (9 am, 12 pm)
- degree of cloud coverage (30%, 60%),
- wind direction (North, South, East, and West),
- and wind speed (5 m/s,10 m/s).

The simulations start with five minutes of clear sky conditions before the cloud field arrives. This time was required in each case to reach an approximately stationary condition. In addition to the arrival of the cloud field and the drop in flux density, clearing represents at least as great a challenge for the receiver and the control system, since there is a risk of exceeding operating limits due to the increase in flux density. Therefore, at the middle of the simulation period, the direction of motion of the cloud field is reversed to resolve the clouds. Regarding the validity of the test, no negative effects are expected due to the unnatural cloud motion.

27 February 2024 08:50:56

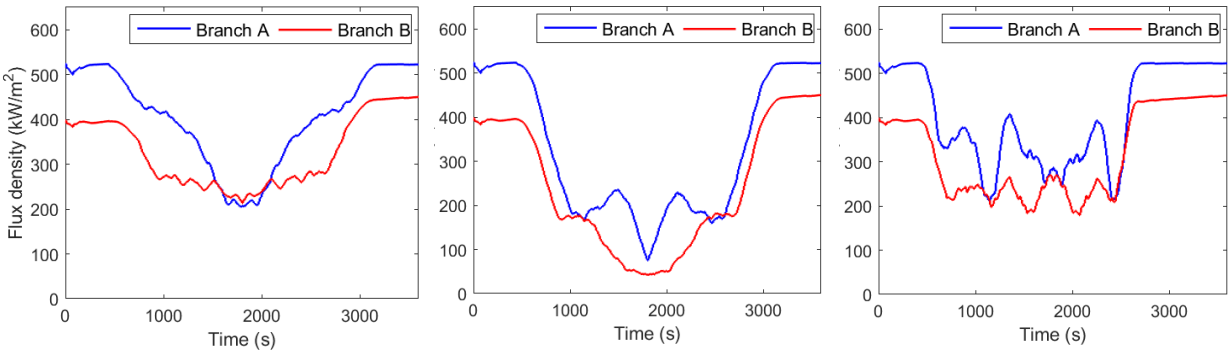

FIGURE 3. Averaged incident flux density on the receiver branches with simulation start at 9 am, different cloud coverage ratios (CCR) and wind speeds (WS): (a) 30 % CCR, 5 m/s WS, (b) 60 % CCR, 5 m/s WS, (c) 30 % CCR, 10 m/s WS

The earlier day-time affects the amount of the incident flux on the sun-facing side (branch B) due to higher cosine losses of the heliostats. The heliostat aimpoint optimization algorithm choses central target points to reduce the spillage losses, as shown in Fig. 4. On the side away from the sun (branch A), the cosine losses are low and the aimpoint algorithm distributes the target points evenly to limit the flux density peaks. From MPC perspective, the test cases with a non-uniform distribution seem to be more challenging, since they might lead to an increased mismatch of the internal reduced-order model and consequently to slight limit violations.

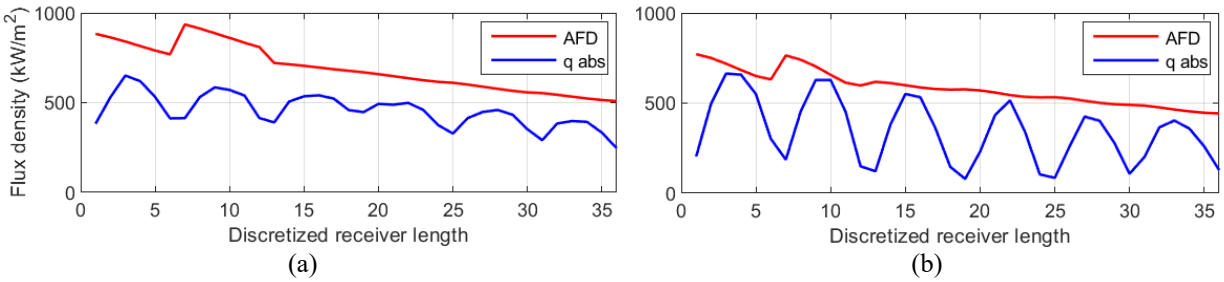

FIGURE 4. Flux density and AFD for a scenario at 9 am in the western branch A (a) and the eastern branch B (b)

A higher velocity of the cloud field leads to faster changes of the flux density, which poses a greater challenge to the controller. The direction of motion of the cloud field determines on which side of the receiver a change in flux density occurs first. Especially for comparison with the conventional PID control this is crucial, since a changed flux density at the cold end of the receiver appears at the feedback path of the controller with a large dead time.

Some of the defined scenarios were not simulated or validated:

- Scenarios with wind direction from north and south represent the extreme values with respect to the dead time. Due to time reasons, scenarios with western and eastern wind direction at 12 pm were not simulated.
- The evaluation of the simulation results showed that the incident irradiation on the receiver at a cloud cover rate of 60 % is partly too low to reach the set point temperature. By setting the mass flow to the minimum value, local hotspots in the film temperatures are likely to evolve. Due to its model predictive character, the MPC detects these safety critical cases and can counteract at an early stage by increasing the mass flow. It has further been shown that in these situations the simulation of the reference model in Dymola becomes unstable and the film temperatures quickly rises to almost 1000 °C. These scenarios with 60 % cloud cover rate, in which such implausible simulation results mainly occurred, are not considered for the evaluation and comparison of the controllers.

The remaining scenarios, shown in Table 3 provide 24 validation cases due to considering both receiver branches. On this basis, the performances of both control algorithms are evaluated and compared.

27 February 2024 08:50:56

TABLE 3. Parameters of validation scenarios

Index	CCR [%]	wind speed [m/s]	wind direction	day time
1a	30	5	North	9:00 AM
2a		10		
3a	30	5	South	
4a		10		
5a	30	5	East	
6a		10		
7a	30	5	West	
8a		10		
1b	30	5	North	12:00 PM
2b		10		
3b	30	5	South	
4b		10		

RESULTS

The flux on the receiver is precalculated and used as input data for the receiver for both control methods, PID and MPC. Based on the mentioned scenarios, the MPC and the PID controller are compared in terms of control accuracy, compliance with the safe operating limits and energy output. Representatively, Fig. 5 shows the control results for scenario 4a with a wind speed of 10 m/s, which poses a more challenging task for the controllers.

Using the PID controller, the outlet temperature shows an oscillating behavior, due to strong fluctuations of the incident irradiation. Contrary to that, the MPC achieves to keep the control deviation acceptable small by manipulating the mass flow in a more aggressive manner. The only three situations, where the outlet temperature drops significantly is due to avoid violations of film temperature limit or AFD. The lines of absorbed flux densities and AFD get very close, but do not cross, especially at second 2500. The film temperature can also be safely restricted to values below 600 °C, without a large decrease in the outlet temperature. Contrary to that, by using the PID controller the film temperatures violate the steady state and even the transient limit several times. In addition to that, the absorbed flux density violates the AFD twice (marked in red), partially with a very high exceed of 60 % at second 2500. Since the outlet temperature also drops below 510 °C in this situation, the cloud standby mode is activated and forces the mass flow to a high value in order bring the receiver back into a safe operation range. The results for this validation case are summarized in Table 4.

TABLE 4. Control results for scenario 4a in branch A

Criteria	MPC	PID
Control deviation (RMSE)	20.1 °C	22.7 °C
Max. violation of steady states film temperature limit	0 °C	24 °C
Max. violation of AFD	0 %	60 %

Considering all 24 validation cases, the MPC shows an equal superior control behavior, as summarized in Table 5. While the thermal efficiency of the receiver with both controllers is similar, the averaged root mean squared control deviation is almost half that small using the MPC. At the same time, there are no critical violations of the film temperature limit by more than 16 °C. The maximum exceed amounts 6 °C that does not jeopardize safe operation. Moreover, in 79 % of the validated cases there is completely no film temperature violation. Contrary, in 88 % of the cases the PID controller cannot avoid a critical violation by 16 °C. In every case the steady state film temperature limit is violated.

27 February 2024 08:50:56

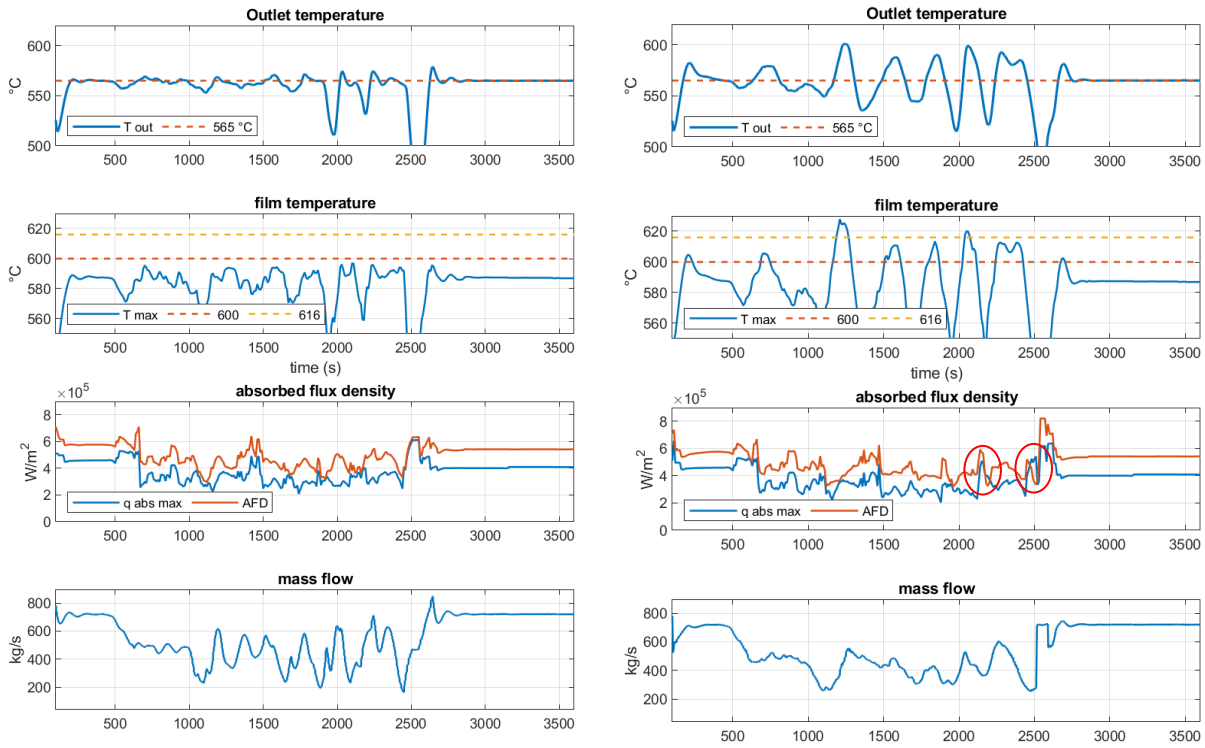

FIGURE 5. Scenario with 30 % cloud coverage, 10 m/s wind speed with direction from north at 9 am on branch A. Using MPC (a) and PID-controller (b), the diagrams show the outlet temperature, film temperatures with steady state and transient limits, absorbed flux density and AFD for locations, where the deviation in the receiver is the smallest, and the mass flow.

The AFD represents a sharp limit. A violation will probably not damage the pipe material instantly, but effects the receiver lifetime. Due to model mismatch in the MPC, the absorbed flux density exceeds the AFD by a maximum amount of 4 %. These violations appear only in branch B for a few seconds due to the non-uniform flux distribution and the higher model mismatch. By slightly increasing the safety margins to the AFD, these violations can be prevented without any expectations of a reduction in control performance. In contrast, this is not possible for the PID controller. Here, the AFD violations reach high values of 28 % in average. Violations of more than 50 % occur in 55 % of the cases validated. This might significantly affect the durability of the receiver.

TABLE 5. Averaged Control results over 24 validation cases

Criteria	MPC	PID
Thermal efficiency	85,97 %	85,96 %
Control deviation (RMSE)	15,3 °C	27,4 °C
Violation of film temperature limits		
Averaged max. violation	0,32 °C	41 °C
Amount of cases (%) > 16 K	0	88 %
0 … 16 K	21 %	12 %
No violations	79 %	0 %
Violation of AFD		
Averaged max. violation	1,5 %	28 %
Amount of cases (%) > 50 %	0 %	55 %
4 … 50 %	0 %	16 %
0 … 4 %	42 %	0 %
No violations	58 %	29 %

27 February 2024 08:50:56

CONCLUSION

This paper addresses the potential of a MPC for its application to a solar tower molten salt receiver, using only the mass flow as manipulated variable. The performance of both controllers was evaluated on 24 simulated validation cases based on different cloud passage scenarios. In general, the MPC maintains the safety boundaries while providing smaller control deviations than the PID controller and an equal thermal efficiency, at the same time. The major advantage of the MPC is that it does not require additional higher-level safety mechanisms, such as a cloud standby mode or a defocus strategy, to detect the critical situations and intervene heuristically. All these interventions are an inherent part of the MPC and are considered in an optimal based way. This means that the receiver can be driven closer to the defined limits for a safe operation and does not have to be controlled so conservatively. Therefore, the set temperature can be increased or even replaced by a cost function that maximizes the outlet temperature to reach even higher temperatures.

ACKNOWLEDGMENTS

The authors gratefully acknowledge the financial support of the German Federal Ministry of Economics and Technology (BMWi), project DynaSalt 2, funding code: 0324202.

REFERENCES

1. H. M. Cekirge and A. Elhassan, “A Comparison of Solar Power Systems (CSP): Solar Tower (ST) Systems versus Parabolic Trough (PT) Systems” in *American Journal of Energy Engineering -2015*, vol. 3, pp. 29-36. doi: 10.11648/j.ajee.20150303.11
2. L. L. Vant-Hull, “The Role of “Allowable Flux Density” in the Design and Operation of Molten-Salt Solar Central Receivers” in *Journal of Solar Energy Engineering-*. vol. 124, pp. 165-169, doi: 10.1115/1.1464124
3. A. Meaburn and F.M. Hughes, “Feedforward control of solar thermal power plants” in *Journal of Solar Energy Engineering -1997*, vol. 119, pp. 52 -60, doi: 10.1115/1.2871838
4. M. Barão, J. M. Lemos and R. Neves-Silva: “Reduced complexity adaptive nonlinear control of a distributed collector solar field” in *Journal of Process Control.* 12. Pages 131-141. doi: 10.1016/S0959-1524(01)00003-8.
5. E. F. Camacho and C. Bordons. “Model Predictive Control”, (Springer-Verlag, second edition, 2004)
6. J. E. Pacheco, “Final Test and Evaluation Results from the Solar Two Project,” Sandia National Laboratories, Albuquerque, New Mexico and Livermore, California, 2002.
7. B. Costa and J. M. Lemos, (2015). “Temperature control of a solar tower receiver based on the Lyapunov method”. In *23th Mediterranean Conference on Control and Automation (MED) –* 2015, Pages 583-588. doi: 10.1109/MED.2015.7158810.
8. B. Belhomme, R. Pitz-Paal, P. Schwarzbözl and S. Ulmer, “A New Fast Ray Tracing Tool for High-Precision Simulation of Heliostat Fields.” in *Journal of Solar Energy Engineering - 2009,* vol. 131, doi 10.1115/1.3139139.
9. R. Flesch, D. Högemann, J. Hackmann, R. Uhlig, P. Schwarzbözl, G. Augsburger and M. Clark, „ Dynamic modeling of molten salt power towers” in *AIP Conference Proceedings 2017*, doi: 1850, 030016, https://aip.scitation.org/doi/abs/10.1063/1.4984359.
10. R. Popp, R. Flesch, T. Konrad, U. Jassmann and D. Abel, "Control-Oriented Model of a Molten Salt Solar Power Central Receiver," in *18th European Control Conference (ECC) - 2019*, pp. 2295-2300, doi: 10.23919/ECC.2019.8795914
11. K. L. Chien, J. A. Hrones, J. B. Reswick: “On the Automatic Control of Generalized Passive Systems*”* in *Transactions of the American Society of Mechanical Engineers -1972*, Vol. 74, pages. 175–185

27 February 2024 08:50:56